Collisional-radiative recombination of Ar^+ ions with electrons in ambient helium at temperatures from 50 K to 100 K

Petr Dohnal,[1] Peter Rubovič,[1] Tomáš Kotrík,[1] Michal Hejduk,[1] Radek Plašil,[1] Rainer Johnsen,[2] and Juraj Glosík[1]
[1]*Department of Surface and Plasma Science, Faculty of Mathematics and Physics, Charles University in Prague, Czech Republic*
[2]*Department of Physics and Astronomy, University of Pittsburgh, Pittsburgh, Pennsylvania 15260, USA*
(Received 26 April 2013; published 29 May 2013)

Ternary electron-assisted collisional radiative recombination (E-CRR) and neutral-assisted radiative recombination (N-CRR) have very strong negative temperature dependencies and hence dominate electron recombination in some plasmas at very low temperatures. However, there are only few data for molecular ions and almost none for atomic ions at temperatures much below 300 K. In this experimental study we used a cryogenic afterglow plasma experiment (Cryo-FALP II) at temperatures from 50 K to 100 K to measure ternary recombination rate coefficients for Ar^+ ions in ambient helium gas. The measured magnitudes and the temperature dependencies of the ternary recombination rate coefficients for electron-assisted and neutral-assisted collisional radiative recombination agree well with theoretical predictions ($K_{\text{E-CRR}} \sim T^{-4.5}$ and $K_{\text{He-CRR}} \sim T^{-2.5}$ to $T^{-2.9}$) over a broad range of electron and He densities.

DOI: 10.1103/PhysRevA.87.052716 PACS number(s): 34.80.Lx, 52.27.Aj, 52.20.−j

I. INTRODUCTION

Electron-ion recombination in cold plasmas can occur by several mechanisms. When the ions in the plasma are molecular, dissociative recombination (DR) [1] is almost always much faster than third-body-assisted recombination, unless the densities of third particles (electrons, ions, and neutrals) are very high or the temperature is very low. Hence, in many afterglow determinations of DR rate coefficients of molecular ions at temperatures near 300 K, neutral densities below $1 \times 10^{17}\,\text{cm}^{-3}$, and electron densities $< 1 \times 10^{10}\,\text{cm}^{-3}$, third-body-assisted recombination can usually be neglected. Experimental methods have now been developed that are capable of measuring DR rate coefficients at the very low temperatures (near 50 K) that exist in cold interstellar clouds. At those temperatures, third-body-assisted recombination becomes competitive with DR and must be clearly separated from binary DR. The studies described here test existing theories of ternary recombination at very low temperatures in helium-buffered plasmas containing predominantly atomic argon ions, thus largely eliminating DR. The remaining recombination processes consist of ternary recombination in which electrons and helium atoms act as third bodies and a slow conversion of atomic argon ions to molecular Ar_2^+ ions that recombine by DR. As will be shown, the relative contributions of the three mechanisms can be separated and the results confirm theoretical calculations.

In the following we will refer to ternary electron-assisted collisional radiative recombination (see, e.g., [2]) as E-CRR and to the ternary neutral-assisted recombination process (see, e.g., [3]) as N-CRR, where N denotes the neutral atom (e.g., He). The overall reaction equations for atomic argon ions in the presence of electrons and helium atoms can be written as

$$\text{Ar}^+ + e^- + e^- \xrightarrow{K_{\text{E-CRR}}} \text{Ar} + e^- \tag{1}$$

and

$$\text{Ar}^+ + e^- + \text{He} \xrightarrow{K_{\text{He-CRR}}} \text{Ar} + \text{He}, \tag{2}$$

where $K_{\text{E-CRR}}$ and $K_{\text{He-CRR}}$ are ternary recombination rate coefficients (in units of $\text{cm}^6\,\text{s}^{-1}$). Writing the reactions in this form is not meant to imply that a single three-particle collision completes the recombination. In general, several energy-reducing collisions are required to render the product atom stable against reionization. Both E-CRR and N-CRR have been extensively treated by semiclassical theories (see, e.g., [2,4]) that solve the coupled equations for three-body electron capture into discrete Rydberg states, ionization, and stepwise collisional and radiative reduction of the electron energy. Results of numerical calculations of E-CRR by Stevefelt *et al.* [2] can be expressed by the following formula for the effective binary rate coefficient:

$$\alpha_{\text{E-CRR}} = 3.8 \times 10^{-9} T_e^{-4.5} n_e + 1.55 \times 10^{-10} T_e^{-0.63} + 6 \times 10^{-9} T_e^{-2.18} n_e^{0.37}\ \text{cm}^3\,\text{s}^{-1}, \tag{3}$$

where T_e is the electron temperature in K and n_e is the electron number density in cm^{-3}. At low temperatures the second and third terms on the right-hand side tend to be small in comparison with the first term and one can define a three-body rate coefficient $K_{\text{E-CRR}}$ by dividing E-CRR by the electron density:

$$K_{\text{E-CRR}} = \alpha_{\text{E-CRR}}/n_e \cong 3.8 \times 10^{-9} T_e^{-4.5}\ \text{cm}^6\,\text{s}^{-1}. \tag{4}$$

Recently, Pohl *et al.* [5] have revised the rates of electron capture into high Rydberg states and of the energy exchange between high Rydberg states and free electrons. In the limit of small energy transfer the revised rates differ drastically from the earlier rates, however, the steady-state recombination rate is only weakly affected. The numerical coefficient in Eq. (4) is reduced to 2.77×10^{-9}. The only experimental data on E-CRR for temperatures below 300 K are those of our Cryo-FALP I studies of Ar^+ ions [6] at 77–180 K, and our recent study at temperatures 57–200 K [7]. Those agreed well with theory. However, our studies of the recombination of H_3^+ and D_3^+ ions with electrons gave no indication of E-CRR, a rather puzzling result since E-CRR should have been faster than binary dissociative recombination at very low temperatures [8–10]. Those observations motivated us

to conduct the present studies of E-CRR in a range of temperatures that is largely unexplored. Ternary recombination in cold and ultracold plasmas is also of interest in the formation of antihydrogen [5,11].

As a consequence of the small electron-to-neutral mass ratio, transfer of electronic energy to heavy particles is slow and N-CRR is less efficient than E-CRR by many orders of magnitude. A good estimate of the recombination rate coefficient can be derived from the energy-diffusion model [3,12–14] that treats the electron energy states as a continuum, as discussed in great detail by Flannery [3]. Flannery derived the following rate coefficient for the case of atomic ions in their parent gas:

$$\alpha_{\text{N-CRR}} = 8\pi \frac{m_e}{M_{\text{atom}}} R_0 R_e^2 \left(\frac{8k_B T_e}{\pi m_e}\right)^{1/2} \sigma_{e,\text{atom}} n_{\text{atom}}. \quad (5)$$

Here, k_B is the Boltzmann constant, m_e and M_{atom} denote the masses of the electron and gas atoms (e.g., helium), $\sigma_{e,\text{atom}}$ is the electron-atom momentum transfer cross section, and $R_e = e^2/k_B T_e (=5.6 \times 10^{-6}$ cm at 300 K). R_0 is a "trapping radius," the assumption being made that electrons that collide with an atom inside this radius recombines with unit probability, while those colliding outside that radius will escape recombination. If R_0 is taken as $2R_e/3$, the recombination coefficient decreases with temperature as $T_e^{-2.5}$ and agrees with the energy-diffusion model of Pitaevskii [12].

The more elaborate theory of Bates and Khare [4], in which recombination proceeds by stepwise collisional deexcitation of excited Rydberg states of the ion, yields nearly identical recombination coefficients (for He^+ in He) at temperatures below 125 K, but lower values (by approximately a factor of 2) at 300 K. Much larger values ($\sim 10^{26}$ cm^6 s^{-1} at 300 K) have been calculated by Whitten *et al.* [15], but, as has been pointed out by Wojcik and Tachiya [13,14], the results of Whitten *et al.* depend sensitively on several assumptions, for instance, that the Rydberg populations of states with binding energies less than $4k_B T$ are in thermal equilibrium.

It is not quite clear how the theoretical results should be modified when the ions and neutrals have different masses, the case of interest in our experiments. Bates and Khare [4] suggest that the recombination rate at low temperatures and densities is approximately proportional to the reciprocal of the ion-atom reduced mass, i.e., that the mass M_{atom} in Eq. (5) should be replaced by $2M_{\text{red}}$, where M_{red} is the reduced mass of the ion and gas atoms. If one adopts that rule, the recombination of Ar^+ ions in helium should be slower by a factor of 0.54 than that for He^+ in helium. This scaling agrees with the conclusion of Wojcik and Tachiya [13,14] that the energy-diffusion model for heavy ions yields smaller rates by a factor of 2 than for ions of the same mass as the gas atoms.

In the case of recombination of atomic argon ions in ambient helium of density [He] Eq. (5) reduces to

$$\alpha_{\text{He-CRR}}(T_e) = 1.2 \times 10^{-27} (T_e/300)^{-2.5} [\text{He}]\ \text{cm}^3\ \text{s}^{-1}. \quad (6)$$

The momentum transfer cross section for electron-helium collisions was taken as 5.4×10^{-16} cm^2 [16], independent of energy.

The ternary rate coefficient $K_{\text{He-CRR}}$ is obtained by dividing $\alpha_{\text{He-CRR}}$ by the helium number density:

$$K_{\text{He-CRR}} = \alpha_{\text{He-CRR}}/[\text{He}]\ \text{cm}^6\ \text{s}^{-1}. \quad (7)$$

Experimental data on ternary neutral-assisted recombination N-CRR at temperatures $\geqslant$300 K have mostly confirmed theoretical predictions [3,4], including the expected $T^{-2.5}$ temperature dependence. Deloche *et al.* [17] found similar coefficients for both atomic and molecular ions. The only experimental measurements at low temperatures (77–150 K) by Cao and Johnsen [18] yielded rate coefficients close to those expected for atomic ions, even though the ions were most likely simple diatomic ions (N_2^+,O_2^+,NO^+). On the other hand, our recent low-temperature studies of recombination of H_3^+ and D_3^+ ions, summarized in [9,10,19–23], gave much faster ternary He-assisted recombination with rate coefficients $K_{\text{He-CRR}}(300\ \text{K}) > 10^{-25}$ cm^6 s^{-1}, indicating that ternary recombination of H_3^+ and D_3^+ ions can also proceed by dissociation of long-lived intermediate rotationally excited H_3^* and D_3^* Rydberg molecules.

In this paper, after describing the Cryo-FALP II apparatus, methods of data analysis, and test measurements on O_2^+ ions, we will discuss the determination of the electron temperature in the afterglow plasma by monitoring the decay of the electron density due to ambipolar diffusion. Finally we will present new data on ternary electron- and helium-assisted recombination of Ar^+ at temperatures down to 50 K.

II. EXPERIMENTS

A. Experimental apparatus

The recombination measurements described here were carried out in a decaying fast-flowing plasma, created by passing helium gas through a continuous microwave discharge and converting the primary active particles (mainly helium metastables) to argon ions by adding argon through a gas inlet downstream from the discharge. When the decay of the electron density is monitored by a Langmuir probe, a thin tungsten wire, the technique is referred to as the flowing afterglow Langmuir probe (FALP) method. Afterglow optical emissions from the decaying plasma, for instance, argon emission lines resulting from recombination, are present but were not analyzed in these experiments. While the FALP method has been used extensively to study recombination in decaying plasmas, the extension to very low temperatures required construction of the Cryo-FALP II apparatus to be described below. Also, additional efforts are needed to characterize the thermal properties of the plasma.

We note in passing that it might have been simpler to construct a cryogenic pulsed "stationary afterglow." However, the FALP arrangement offers better control of plasma parameters and avoids exposing all reagent gases directly to an intense discharge, which can lead to undesired excitation of atomic or molecular species.

In the Cryo-FALP II apparatus (see Fig. 1) the reaction section of the flow tube can be cooled down to 40 K and recombination processes can be studied down to 50 K. Effective binary recombination rate coefficients above 1×10^{-8} cm^3 s^{-1} can be reliably measured. A very broad range of helium pressures and partial pressures of reactant gases

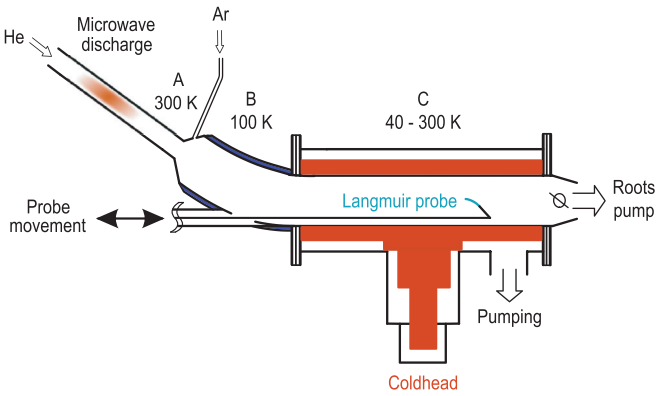

FIG. 1. (Color online) Simplified diagram of the Cryo-FALP II apparatus (not to scale). The three sections A, B, and C have temperatures of 300, 100, and 40–300 K, respectively. The axially movable Langmuir probe measures the decaying electron density along the section C of the flow tube.

can be covered which enables accurate measurements of rate coefficients of binary and ternary recombination processes. Using Cryo-FALP II we recently studied E-CRR of Ar^+ at temperatures 57–200 K and at electron number densities $n_e \sim 10^9 - 10^{10}$ cm^{-3} [6,7] and we found good agreement with theoretical predictions (see, e.g., [2]). At those electron densities E-CRR of Ar^+ was the dominant loss process during the afterglow. The present work focuses mainly on He-assisted ternary recombination (He-CRR) of Ar^+ ions at very low temperatures and lower electron densities. However, the relative contributions of E-CRR and He-CRR are often of similar magnitude and the data analysis (see Sec. II B) necessarily involves both processes.

A detailed description of the FALP technique can be found in the papers by Mahdavi [24] and by Smith [25] and in the book by Larsson and Orel [1]. The high-pressure version of the FALP and Langmuir probe technique is described in [26]. A short description of Cryo-FALP II is also given in Refs. [7,22,23].

The flow tube of Cryo-FALP II has three sections A, B, and C with different temperatures. The internal diameter of the flow tube is ~5 cm and the length is ~80 cm. Helium buffer gas flows through the glass section (A, 300 K) where it is partially ionized in a microwave discharge (2.45 GHz, power of 10–30 W). Downstream from the discharge the plasma contains mainly helium metastables (He^m), He^+ ions, and electrons. At high helium densities ([He] $\sim (1-25) \times 10^{17}$ cm^{-3}) most He^+ ions are converted by ternary association to He_2^+. The addition of Ar gas ([Ar] $\sim (0.01-10) \times 10^{14}$ cm^{-3}) further downstream from the discharge region at the beginning of the stainless steel section B of the flow tube converts the He_2^+ ions by charge transfer reaction to Ar^+ ions. The metastables He^m are converted to Ar^+ ions by Penning ionization [27,28]. The Ar^+-dominated plasma is carried along the section B of the flow tube that is cooled to ~100 K by liquid nitrogen. In sections A and B at temperatures above 100 K the recombination of He_2^+ and Ar^+ ions is very slow and the plasma decay is caused mainly by ambipolar diffusion to the walls of the flow tube.

After precooling in section B the plasma enters section C, made from stainless steel. This section is connected to the cold head (Sumitomo CH-110) by copper braids, and temperatures of the flow tube wall in the range of 40–300 K can be achieved. To obtain good thermal insulation the whole section C and the cold head are placed in another vacuum chamber. Calculations showed that the buffer gas temperature T_{He} in section C is equal to the wall temperature T_W of the flow tube, and that the ion and electron temperatures (T_{ion} and T_e, respectively) in the afterglow are equal to that of the buffer gas, i.e., $T_{ion} = T_e = T_{He} = T_W$. The temperature distribution along the flow tube and the resulting temperature of the He buffer gas was calculated by a computer model (see [7]). The calculated relaxation time constant for the electron temperature is <0.1 ms, i.e., electron temperature relaxes to the buffer gas temperature immediately after removal of the He metastables (see [26,29]). We verified the electron thermalization by analyzing characteristic times of ambipolar diffusion (see Sec. II D). The results supported the assumption $T_W = T_e$. The ion thermalization is many times faster (with time constant < 0.1 μs) because the masses of ions are similar to those of the neutral atoms. This was also confirmed by spectroscopic measurements in H_3^+- and D_3^+-dominated plasma at otherwise very similar conditions (see [8–10]). In the following we will refer to the kinetic temperatures simply as T without subscripts.

The gas handling system and the flow tube itself employ UHV technology and high-purity He and Ar are used. Helium is further purified by passing it through two in-line liquid-nitrogen-cooled molecular sieve traps, resulting in an estimated level of impurities of the order of 10^{-2} ppm. A throttle valve at the downstream end of the flow tube (prior to the Roots pump) adjusts the working pressure and the flow velocity of the buffer gas to the desired values.

The recombination measurements, carried out in section C of the flow tube, rely on the electron density decays as determined by an axially movable Langmuir probe (length 7 mm, diameter 18 μm). To convert positions in the flow tube to afterglow time, the plasma velocity is needed. It is measured by modulating the discharge and observing the time of the Langmuir probe response at certain positions on the flow tube axis. The plasma velocities range from 1 to 20 m s^{-1}, depending on pressure, helium flow rate, and on the flow tube temperature (see Fig. 2 in [7]). The plasma velocity is not constant along the whole flow tube because the wall temperature is different in different sections.

The Langmuir probe characteristics are measured point by point along the flow tube, and the actual values of the electron densities are obtained from the saturated electron current to the probe at positive probe potential [30,31]. The reliability of Langmuir probes used in this mode has been established many times, e.g., by comparing recombination rate coefficients obtained with laser absorption spectroscopy (CRDS technique [32]) to those obtained with Langmuir probes [8–10] or by measuring recombination rate coefficients of well-known recombination processes, e.g., dissociative recombination of O_2^+ ions with electrons (see Sec. II C).

To establish optimal conditions for the measurements of the ternary rate coefficients we developed a kinetic model which includes all significant processes taking place during the

afterglow [33,34]. The temperature evolution along the flow tube was explicitly taken into the account. The calculations show that Ar^+ is the dominant ion at the beginning of the section C, and that the plasma is completely thermalized at that position.

B. Data analysis and conditions of measurement

In a quasineutral afterglow plasma, dominated by a single ion species A^+ in ambient helium gas, the loss rate of electrons and ions is given by

$$\frac{dn_e}{dt} = \frac{d[A^+]}{dt} = -\alpha_{\text{bin}}[A^+]n_e - K_{\text{He-CRR}}[\text{He}][A^+]n_e - K_{\text{E-CRR}}[A^+]n_e^2 - \frac{n_e}{\tau_D} - \frac{n_e}{\tau_R}, \quad (8)$$

where α_{bin} is the rate coefficient of binary recombination (e.g., DR) and τ_D is the time constant of ambipolar diffusion. The additional term containing time constant τ_R accounts for a loss due to possible reactions (for details see Sec. II D). By combining the recombination terms into an effective binary rate coefficient α_{eff} and combining the diffusion and reaction loss terms into a linear loss term characterized by a time constant τ_L one obtains

$$\frac{dn_e}{dt} = \frac{d[A^+]}{dt} = -\alpha_{\text{eff}}n_e^2 - \frac{n_e}{\tau_L}, \quad (9)$$

where

$$\alpha_{\text{eff}}(T,[\text{He}],n_e) = \alpha_{\text{bin}} + K_{\text{He-CRR}}[\text{He}] + K_{\text{E-CRR}}n_e \quad (10)$$

and

$$\frac{1}{\tau_L} = \frac{1}{\tau_D} + \frac{1}{\tau_R}. \quad (11)$$

We note that a linear addition of the contributions of He-CRR and E-CRR in Eq. (8) is not necessarily correct, as Bates pointed out [35], since both processes can partly compete for the populations of the same energy levels. Hence, we regard Eq. (10) as a first (linear) approximation that is valid only in the limit when a small fraction of the intermediate levels is stabilized by collision with electrons or neutrals. We will discuss this again in Sec. IV.

The effective binary recombination rate coefficients for ternary processes depend on electron and neutral density. For atomic Ar^+ ions purely binary recombination can be neglected so that the overall effective (measured) binary rate coefficient can be taken as $\alpha_{\text{eff}} = \alpha_{\text{E-CRR}} + \alpha_{\text{He-CRR}} = K_{\text{E-CRR}}n_e + K_{\text{He-CRR}}[\text{He}]$. Different experimental conditions must be chosen to separate the two contributions: To determine $K_{\text{E-CRR}}$, n_e should be large but [He] should be small. On the other hand, to determine $K_{\text{He-CRR}}$, [He] should be as high as possible, while n_e should be small. Figure 2 shows decay curves measured at a temperature of 60 K for two different sets of parameters. For the decay curve (i) [He] was minimized and n_e maximized, so that E-CRR dominates. For the decay curve (ii) [He] was maximized and n_e minimized, so that He-CRR dominates. The temperature distribution model showed that for both data sets in Fig. 2 the temperature in the recombining plasma is relaxed to 60 ± 2 K. This was confirmed by measuring the plasma velocity along the flow tube [7].

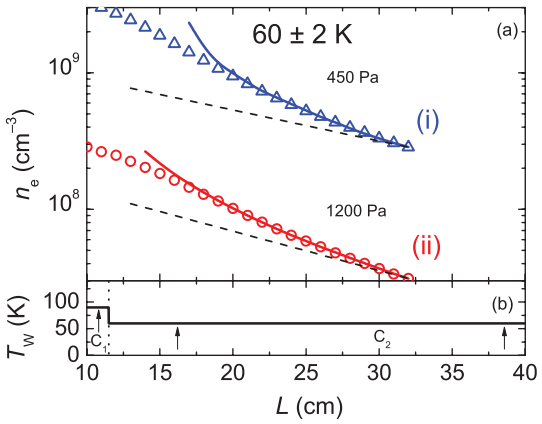

FIG. 2. (Color online) (a) Measured electron density decay in an Ar^+-dominated afterglow plasma for two helium pressures, 450 (open triangles) and 1200 Pa (open circles). Symbols show measured data, full lines represent fits of these data, and dashed lines indicate diffusion losses. The effective recombination rate coefficients at 1200 and 450 Pa are 1.0×10^{-7} and 3.3×10^{-8} cm^3 s^{-1}, respectively. (b) Measured temperatures of the flow tube wall (T_W) at the positions of the temperature sensors (indicated by arrows). Section C is divided into two subsections C_1 and C_2 in the figure indicating different measured temperature.

In a low-temperature Ar^+-dominated plasma in He buffer gas with a small admixture of Ar gas the reactive loss term in Eq. (8) accounts for the relatively slow ternary association of Ar^+ with atomic argon, i.e., the reaction $Ar^+ + Ar + He \longrightarrow Ar_2^+ + He$ [36,37]. Since the Ar_2^+ product ions recombine rapidly with electrons [1,38], the rate determining step at low argon concentrations is ternary association. The association reaction essentially constitutes an additional electron loss process that can be represented by a time constant τ_R as written in Eq. (8). In this particular case, τ_R depends on the ternary association rate coefficient k_a and on Ar and He densities, $\tau_R = 1/(k_a[\text{Ar}][\text{He}])$. The temperature dependence of τ_R is given by the temperature dependence of k_a (details will be discussed below). At higher Ar and He densities and lower temperatures the formation of Ar_2^+ is faster and the recombination of Ar_2^+ is the rate determining process. The effect of Ar_2^+ ions on observed effective binary recombination (on α_{eff}) was determined by measuring the effective binary recombination rate coefficient as a function of argon density. Examples of such dependencies are plotted in Fig. 3 for 62 K and He pressure 500 and 1200 Pa. The measured effective binary recombination rate coefficients are constant below $[\text{Ar}] = 1 \times 10^{13}$ cm^{-3} but increase above this value, in accordance with our kinetics model that includes the formation of Ar_2^+. To minimize the influence of Ar_2^+ formation on the measured α_{eff} the typical number density of Ar used in the present experiment was limited to $[\text{Ar}] \sim 3 \times 10^{12}$ cm^{-3}, which is still sufficient to form an Ar^+-dominated plasma before entering zone C of the flow tube. The final data were taken under conditions where the effect of Ar_2^+ on measured α_{eff} was negligible.

Figure 4 shows data for α_{eff} as a function of helium density [He] for three different temperatures. The slopes of the linear dependencies yield $K_{\text{He-CRR}}(T)$ [see Eq. (10)], and the

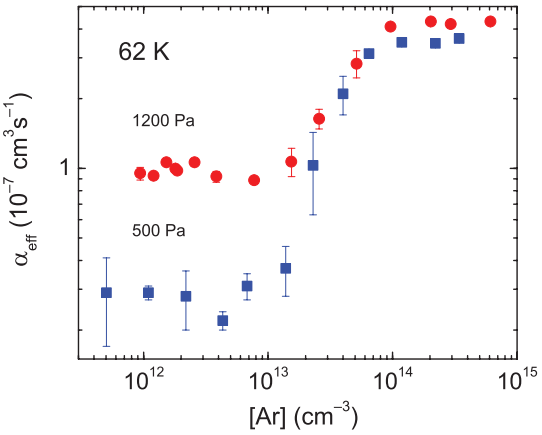

FIG. 3. (Color online) The dependence of measured effective binary recombination rate coefficient α_{eff} on Ar number density at 62 K and indicated pressures of He (full circles for the pressure of 1200 Pa and full squares for 500 Pa). Displayed errors are statistical.

intercept at [He] = 0 gives the sum $\alpha_{bin} + K_{E\text{-}CRR} n_e$. Since previous work [6] has shown that $\alpha_{bin} = 0$ (see Fig. 4 and discussion in [6]), we can write $\alpha_{eff} = K_{E\text{-}CRR} n_e$ at [He] = 0. This is in agreement with the expectation of slow radiative recombination of atomic Ar^+.

C. Test measurements on recombination of O_2^+ ions

Some of the present studies were conducted under conditions (helium densities, temperatures, flow velocities, etc.) that have not been used much in earlier work. Also, the data analysis relies on modeling of the temperature distribution and flow velocities. As a precaution, we performed a series of test measurements of the well-known binary recombination rate coefficient of dissociative recombination $\alpha_{bin\ DR}$ of O_2^+ ions, which is much simpler to measure than ternary recombination. Our test results (see Fig. 5) agreed very well with previous data [39–45]. The rate coefficients were measured for three temperatures and over a broad range of He pressures and O_2

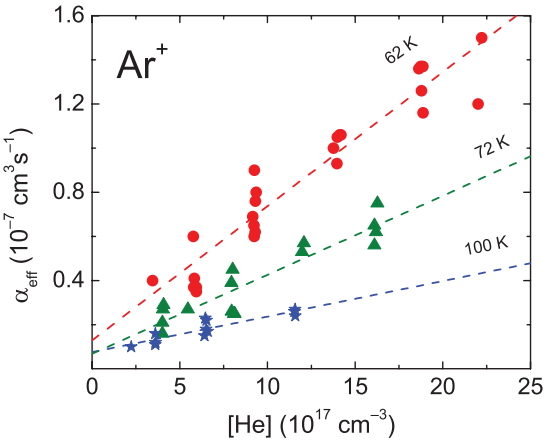

FIG. 4. (Color online) Measured dependence of the effective binary recombination rate coefficient $\alpha_{eff}(T, [He], n_e)$ of recombination of Ar^+ ions with electrons on He number density at 62 (full circles), 72 (full triangles), and 100 K (full stars). The lines represent the linear fits of the data.

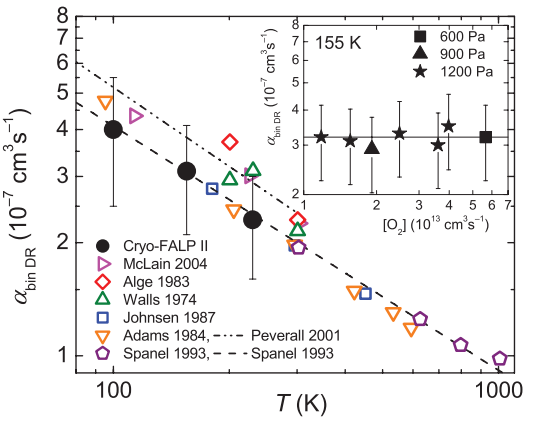

FIG. 5. (Color online) Temperature dependence of the measured recombination rate coefficient $\alpha_{bin\ DR}$ of the binary dissociative recombination of O_2^+ ions with electrons. The present Cryo-FALP II data (large circles) are compared to previous results [39–45]. The dashed line represents a fit given by [43,45]. Inset: Data obtained at different O_2 number densities, measured at 155 K and at several helium pressures. The full line is the mean of the measured values.

number densities. The results of these tests clearly confirm the validity of the methods used in present experiments.

D. Verification of the electron temperature by measuring ambipolar diffusion losses

The strong temperature dependencies of $K_{E\text{-}CRR}$ and $K_{He\text{-}CRR}$ make the electron temperature a crucial parameter that is not directly measured, but within some limitations a precise measurement of ambipolar diffusion losses in the late afterglow can serve as a "diffusion thermometer." Ambipolar diffusion losses also enter directly [see Eq. (8)] in the determinations of α_{eff} and τ_L. The measured time constant τ_L has two components: one representing ambipolar diffusion (τ_D) and the second representing reactive losses (τ_R) (see Sec. II B). The value of τ_D depends on temperature, helium density, the characteristic diffusion length Λ of the flow tube, and the zero-field reduced mobility K_0 of Ar^+ ions in He (for details see [6]). For a long flow tube of radius R the characteristic diffusion length is $\Lambda = R/2.405$. Using the relations given by Mason and McDaniel [46] one can show that if electrons, ions, and gas atoms have the same temperature $T_e = T_{ion} = T_{He} = T$ then

$$\frac{1}{\tau_D} = 4.63 \times 10^{15} \frac{K_0(T)}{\Lambda^2} \frac{T}{[He]}\ s^{-1}. \qquad (12)$$

The units are [He] in cm^{-3}, T in K, Λ in cm, and K_0 in $cm^2\ V^{-1}\ s^{-1}$. Since the zero-field reduced mobility of Ar^+ in He is nearly constant for temperatures below 300 K, a graph of $[He]/\tau_D$ versus T should yield nearly a straight line, with small deviations when the dependence of K_0 on temperature is included [6]. Measured values of $[He]/\tau_D$ should be proportional to the temperature thus providing an independent measure of the otherwise difficult to determine electron temperature. Figure 6 shows the theoretical temperature dependence of $[He]/\tau_D$, where τ_D is calculated using zero-field reduced mobilities of $K_0 = 18.9\ cm^2\ V^{-1}\ s^{-1}$

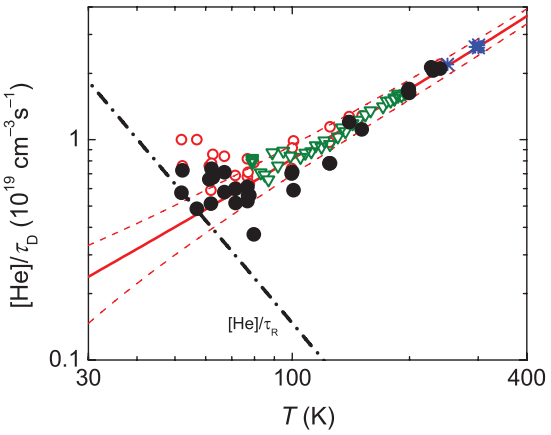

FIG. 6. (Color online) Temperature dependencies of the inverted time constants of diffusion losses $[He]/\tau_D$ and $[He]/\tau_R$. Solid line represents the theoretical temperature dependence of $[He]/\tau_D$ on T, calculated from the zero-field reduced mobility of Ar^+ in He for a thermalized afterglow plasma [47–49]. Dashed lines are calculated for 10 K higher or lower temperatures. The dash-dotted line labeled $[He]/\tau_R$ shows values corresponding to reactive losses due to Ar_2^+ formation at densities $[Ar] = 3 \times 10^{12}$ cm^{-3} and $[He] = 7 \times 10^{17}$ cm^{-3} (see text). In the calculation we used the formula $[He]/\tau_R = k_a[Ar][He]^2 = 9.5 \times 10^{-32}(300/T)^{2.19}[Ar][He]^2$. Data measured with Cryo-FALP I (open triangles) are adapted from [6] as well as data indicated by asterisk symbols measured at 250 and 300 K. Open circles indicate measured $[He]/\tau_L$ and closed circles indicate corresponding experimental $[He]/\tau_D$ calculated for particular [He] and [Ar] using relation $[He]/\tau_D = ([He]/\tau_L - [He]/\tau_R)$.

at 77 K and 20.5 cm^2 V^{-1} s^{-1} at 300 K [47–49] and a linear interpolation at intermediate temperatures.

To show the sensitivity to small errors in temperature, we also include in Fig. 6 calculated values of $[He]/\tau_D$ for two temperatures that are 10 K higher or lower. As may be seen in Fig. 6, the accuracy of the "diffusion thermometer" deteriorates rapidly below ~70 K because the experimental values $[He]/\tau_L$ include a contribution $[He]/\tau_R$ due to reactive losses in the late afterglow [see Eq. (11)]. We tried to correct the raw "experimental" values $[He]/\tau_L$ (open circles) by subtracting an estimated reactive loss term $[He]/\tau_R$ to obtain the pure diffusion loss rate term $[He]/\tau_D$ (solid circles). The reactive loss term $[He]/\tau_R$ was ascribed to conversion of Ar^+ ions to fast recombining Ar_2^+ ions, using the experimental association ternary rate coefficient k_a of Bohme *et al.* [36] and extrapolating it assuming a temperature dependence of the form $k_a \sim T^{-n}$. From the measured values $k_a(82\text{ K}) = 1.6 \times 10^{-30}$ cm^6 s^{-1} and $k_a(290\text{ K}) = 1 \times 10^{-31}$ cm^6 s^{-1} we calculated $k_a(T) = 9.5 \times 10^{-32}(300/T)^{2.19}$ cm^6 s^{-1}. The size of this correction is included in Fig. 6 (dash-dotted line), the values were calculated for $[Ar] = 3 \times 10^{12}$ cm^{-3} and $[He] = 7 \times 10^{17}$ cm^{-3}. Since the reactive losses increase rapidly at lower temperatures, while the diffusion losses become smaller, the accuracy of the diffusion thermometer becomes poor below 70 K and corrections for reactive losses do not improve it by much. For comparison, in Fig. 6 we also show data from our previous FALP and Cryo-FALP I experiments measured at 250 and 300 K [6]. In that case the whole flow tube was cooled

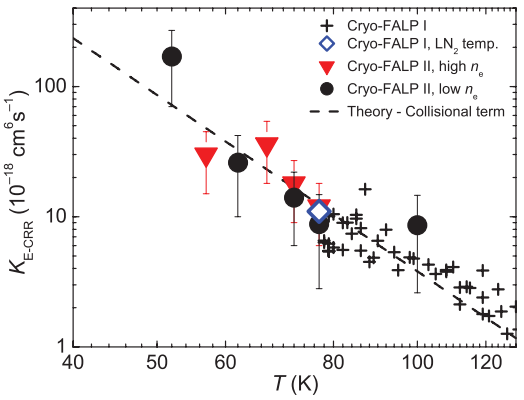

FIG. 7. (Color online) Temperature dependence of the measured ternary recombination rate coefficient $K_{E\text{-}CRR}$ of ternary electron-assisted collisional radiative recombination of Ar^+ ions with electrons. The full circles are the present data measured at lower $n_e(10^8-10^9$ cm$^{-3})$. The data represented by full triangles are measured in our previous studies at higher $n_e(10^9-10^{10}$ cm$^{-3})$ [7]. Data depicted by the open rhomboid at 77 K is compiled from several measurements on Cryo-FALP I. The crosses indicate previous data measured on Cryo-FALP I at temperatures above 77 K (adopted from [6]). The dashed line indicates $K_{E\text{-}CRR}$ calculated by using Stevefelt's formula (4), $K_{E\text{-}CRR} \sim T^{-4.5}$.

by liquid nitrogen to the same temperature and there was no doubt about temperature equilibration.

The measurements of the diffusion losses corroborate our calculations of the temperature distribution in the flow tube only for temperatures above ~70 K. Nevertheless, this does not necessarily imply a difference between T_W, T_e, and T_{ion} below 70 K. The agreement between experimental data on the rate coefficients for E-CRR and N-CRR and theory (see Secs. III A and III B) also supports the assumption of complete thermalization.

III. RESULTS AND DISCUSSION

A. Temperature dependence of $K_{E\text{-}CRR}$

Figure 7 shows the temperature dependence of $K_{E\text{-}CRR}$ obtained in the present experiment and compares it to previous data measured with the Cryo-FALP I apparatus in the range 77–200 K [6], to previous data measured with the Cryo-FALP II apparatus in the range 57–77 K [7], and to theoretical dependence. The agreement between the experimental data sets is good, even though the electron density n_e in the earlier experiments was much higher $(10^9-10^{10}$ cm$^{-3})$ than in the present experiment $(10^8-10^9$ cm$^{-3})$ and experimental conditions were different. In the present study $K_{E\text{-}CRR}$ was obtained by extrapolation of α_{eff} to zero helium density, as shown in Fig. 4. The present and previous data agree well with the collisional term of the Stevefelt formula [see Eq. (4)], leaving no doubt that the $K_{E\text{-}CRR} \sim T^{-4.5}$ dependence remains valid for Ar^+ ions down to 50 K.

The agreement of the experimental values of $K_{E\text{-}CRR}$ with theory can be taken also as another confirmation that the electron temperature and the measured temperature of the wall of the flow tube are nearly equal. Note also the good agreement

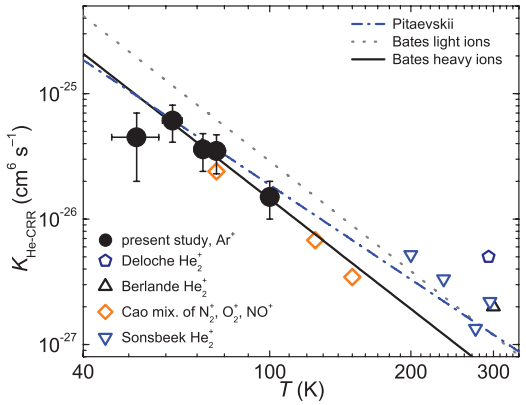

FIG. 8. (Color online) Temperature dependence of the measured ternary recombination rate coefficient $K_{\text{He-CRR}}$ of He-assisted recombination of Ar^+ ions with electrons (full circles). Included are also data from previous experiments [17,18,50,51]. The dotted line follows calculation by Bates [4]; the solid line is scaled for this study using the dependence of the ternary recombination rate coefficient on reduced mass as suggested by Bates [4]. The dash-dotted line indicates theory by Pitaevskii [12].

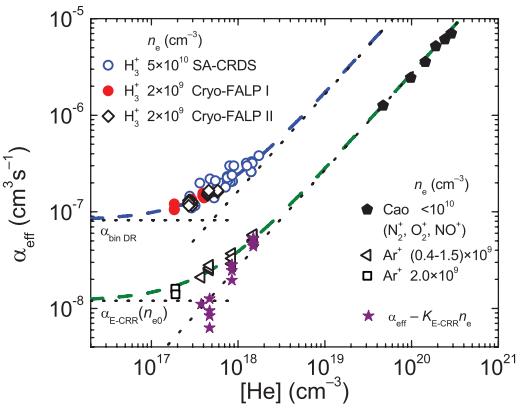

FIG. 9. (Color online) Dependence of the effective recombination rate coefficient α_{eff} on helium number density at 77 K. Present values (open triangles) are plotted together with values obtained by Cao *et al.* [18] (full pentagons) for a mixture of ions, by Varju *et al.* [8], by Dohnal *et al.* [9], and by Glosik *et al.* [19] for H_3^+ and by Kotrik *et al.* [6] for Ar^+ (open squares). The full stars are the present data corrected by subtracting the E-CRR component of α_{eff}. The dashed lines are linear fits to the data (values by Cao were not included in the fit). The dotted lines show the binary and the ternary components of the fitted α_{eff}.

of data obtained at 77 K at very different experimental conditions (it will be again discussed in Sec. IV).

B. Temperature dependence of $K_{\text{He-CRR}}$

The measured temperature dependence of $K_{\text{He-CRR}}$ of ternary recombination of Ar^+ ions with electrons in helium buffer is depicted in Fig. 8, together with examples of data measured in previous experiments with different ions at higher temperatures, predominantly at 300 K [17,18,50,51]. Our data for Ar^+ ions agree well with the calculations of Bates [4] after scaling by the reduced mass factor. The temperature dependence (approximately $T^{-2.9}$) is somewhat stronger than the $T^{-2.5}$ dependence of Pitaevskii [12], presumably because the energy diffusion model of Pitaevskii ignores the discreteness of the electron energy states.

IV. DISCUSSION AND CONCLUSIONS

We have reported on He-assisted ternary recombination of atomic ions below 300 K and rate coefficients of both ternary recombination processes were clearly separated and measured in a well-characterized afterglow plasma at temperatures below 100 K. Careful attention was paid to verifying electron temperatures by measuring the characteristic time constant of ambipolar diffusion τ_D at fixed pressure and flow tube temperature. It was concluded that the plasma particles have nearly the same temperature as the wall of the flow tube, i.e., that $T = T_e = T_{\text{ion}} = T_{\text{He}} = T_W$. However, at the lowest temperatures the verification was complicated by reactive losses.

The measured magnitudes and the temperature dependencies of both ternary recombination rate coefficients $K_{\text{He-CRR}}$ and $K_{\text{E-CRR}}$ of Ar^+ ions agree with theoretical predictions [3,4,12] ($K_{\text{He-CRR}} \sim T^{-2.9}$) in the temperature range from 50 to 100 K and $K_{\text{E-CRR}} \sim T^{-4.5}$ in the range from 50 to 180 K [2] over a broad range of electron and He densities. This observed agreement is not at all obvious. Recent experimental studies of both ternary recombination processes for H_3^+ and D_3^+ ions at temperatures below 300 K gave drastically different results [9,10,22,23], as is demonstrated in Fig. 9 that summarizes the effective binary recombination rate coefficients α_{eff} measured at 77 K in helium afterglow plasmas dominated by different ions. The data obtained by Cao *et al.* [18] for a mixture of molecular ions at very high helium densities are in agreement with the aforementioned results, giving comparable ternary rate coefficients. At their experimental conditions the ternary E-CRR and the binary dissociative recombination can be neglected and He-CRR is by far the dominant recombination process.

The figure also shows data obtained for atomic Ar^+ ions in the present experiments for electron densities $n_e = (0.4-1.5) \times 10^9$ cm^{-3} and He densities [He] $= (5-20) \times 10^{17}$ cm^{-3}. Some earlier data measured at high n_e and low [He] [6] are also plotted. For atomic Ar^+ ions binary recombination is negligible and both ternary processes He-CRR and E-CRR have comparable rates. The overall rate coefficients can be expressed as $\alpha_{\text{eff}} = \alpha_{\text{He-CRR}} + \alpha_{\text{E-CRR}} = K_{\text{He-CRR}}[\text{He}] + K_{\text{E-CRR}} n_e$. At high [He] and low n_e (triangles) $\alpha_{\text{He-CRR}}$ dominates, while at low [He] and high n_e (open squares) $\alpha_{\text{E-CRR}}$ dominates. The fit of the Ar^+ data gives values $K_{\text{He-CRR}}$ and $K_{\text{E-CRR}}$ in agreement with those obtained by precise analyses (see Figs. 7 and 8). At low [He] the data (triangles) level off due to the contribution from $\alpha_{\text{E-CRR}}$, indicated by a horizontal dashed line (calculated for $n_e = 1 \times 10^9$ cm^{-3}). To show the contribution from $K_{\text{He-CRR}}$ alone we plotted the values $\alpha_{\text{He-CRR}}$ (indicated by full stars) obtained by subtracting $\alpha_{\text{E-CRR}}$ from the measured α_{eff}. We used expression (4) for $\alpha_{\text{E-CRR}}$ and the actual n_e. Note that the corrected data $\alpha_{\text{He-CRR}}$ (stars) and data obtained by Cao *et al.* [18] (pentagons) then follow a straight line $\alpha_{\text{He-CRR}} = K_{\text{He-CRR}}[\text{He}]$ over three orders of magnitude of [He].

The sample of data (upper set of data) obtained in H_3^+-dominated He buffered afterglow plasma are significantly larger. These data were obtained at electron densities from 2×10^9 up to 5×10^{10} cm^{-3} in Cryo-FALP I, Cryo-FALP II, and SA-CRDS experiments [8,9,19]. We did not observe any significant dependence of α_{eff} on n_e that would indicate electron-assisted recombination (see discussion in [9,10,22,23]), so we can expect $\alpha_{\text{eff}} = \alpha_{\text{bin DR}} + \alpha_{\text{He}} = \alpha_{\text{bin DR}} + K_{\text{He}}[\text{He}]$, where $\alpha_{\text{bin DR}}$ is the binary rate coefficient of dissociative recombination of H_3^+ and K_{He} ternary rate coefficients of helium-assisted recombination of H_3^+. The seeming absence of electron-assisted recombination is surprising (see discussion in [9,10]).

Figure 9 strongly suggests that the mechanisms of the ternary helium-assisted processes for Ar^+ and H_3^+ (D_3^+) must be very different. The rate coefficients at low [He] are also different. They reflect dissociative recombination in the case of H_3^+ ($\alpha_{\text{bin DR}}$) and ternary electron-assisted recombination ($\alpha_{\text{E-CRR}}$) in the case of Ar^+.

The present study was, in part, undertaken to learn whether our earlier measurements of the ternary recombination rate coefficients of H_3^+ and D_3^+ [9,10,19,20,23,52] were subject to possible systematic errors. This does not seem to be the case. The good agreement of the helium-assisted ternary channel for Ar^+ with theory [4] strongly corroborates the methods used in the earlier work. We conclude that the very fast helium-assisted ternary recombination of H_3^+ and D_3^+ ions must be due to an entirely different mechanism than that proposed for atomic ions by Bates and Khare [4] and Flannery [3]; for discussion and suggestion of the mechanism see [9,19–21].

The presented experimental results on the ternary electron- and neutral-assisted recombination of atomic Ar^+ ions at temperatures down to 50 K show a remarkable difference in comparison with ternary recombination of H_3^+ and D_3^+ ions. To find differences between ternary recombination of atomic and molecular ions and a possible dependence on type of buffer gas we plan to study ternary recombination of other ions and temperature dependence of recombination processes at temperatures down to 30 K.

ACKNOWLEDGMENTS

This work was partly supported by GACR 205/09/1183, GACR P209/12/0233, SV 267 302, GAUK 353811, GAUK 388811, and GAUK 659112.

[1] M. Larsson and A. Orel, *Dissociative Recombination of Molecular Ions* (Cambridge University Press, Cambridge, 2008).
[2] J. Stevefelt, J. Boulmer, and J. Delpech, Phys. Rev. A **12**, 1246 (1975).
[3] M. R. Flannery, J. Chem. Phys. **95**, 8205 (1991).
[4] D. Bates and S. Khare, Proc. Phys. Soc. London **85**, 231 (1965).
[5] T. Pohl, D. Vrinceanu, and H. R. Sadeghpour, Phys. Rev. Lett. **100**, 223201 (2008).
[6] T. Kotrik, P. Dohnal, S. Roucka, P. Jusko, R. Plasil, J. Glosik, and R. Johnsen, Phys. Rev. A **83**, 032720 (2011).
[7] T. Kotrik, P. Dohnal, P. Rubovic, R. Plasil, S. Roucka, S. Opanasiuk, and J. Glosik, Eur. Phys. J. Appl. Phys. **56**, 24011 (2011).
[8] J. Varju, M. Hejduk, P. Dohnal, M. Jilek, T. Kotrik, R. Plasil, D. Gerlich, and J. Glosik, Phys. Rev. Lett. **106**, 203201 (2011).
[9] P. Dohnal, M. Hejduk, J. Varju, P. Rubovic, S. Roucka, T. Kotrik, R. Plasil, J. Glosik, and R. Johnsen, J. Chem. Phys. **136**, 244304 (2012).
[10] P. Dohnal, M. Hejduk, P. Rubovic, J. Varju, S. Roucka, R. Plasil, and J. Glosik, J. Chem. Phys. **137**, 194320 (2012).
[11] T. C. Killian, S. Kulin, S. D. Bergeson, L. A. Orozco, C. Orzel, and S. L. Rolston, Phys. Rev. Lett. **83**, 4776 (1999).
[12] L. P. Pitaevskii, Sov. Phys. JETP **1**, 919 (1962).
[13] M. Wojcik and M. Tachiya, J. Chem. Phys. **110**, 10016 (1999).
[14] M. Wojcik and M. Tachiya, J. Chem. Phys. **112**, 3845 (2000).
[15] B. L. Whitten, L. W. Downes, and W. E. Wells, J. Appl. Phys. **52**, 1255 (1981).
[16] R. W. Crompton, M. T. Elford, and R. L. Jory, Aust. J. Phys. **20**, 396 (1967).
[17] R. Deloche, P. Monchicourt, M. Cheret, and F. Lambert, Phys. Rev. A **13**, 1140 (1976).
[18] Y. S. Cao and R. Johnsen, J. Chem. Phys. **94**, 5443 (1991).
[19] J. Glosik, R. Plasil, I. Korolov, T. Kotrik, O. Novotny, P. Hlavenka, P. Dohnal, J. Varju, V. Kokoouline, and C. H. Greene, Phys. Rev. A **79**, 052707 (2009).
[20] J. Glosik, I. Korolov, R. Plasil, T. Kotrik, P. Dohnal, O. Novotny, J. Varju, S. Roucka, C. H. Greene, and V. Kokoouline, Phys. Rev. A **80**, 042706 (2009).
[21] J. Glosik, R. Plasil, T. Kotrik, P. Dohnal, J. Varju, M. Hejduk, I. Korlov, S. Roucka, and V. Kokoouline, Mol. Phys. **108**, 2253 (2010).
[22] P. Rubovič, P. Dohnal, M. Hejduk, R. Plašil, and J. Glosík, J. Phys. Chem. A (2013), doi: 10.1021/jp3123192.
[23] R. Johnsen, P. Rubovič, P. Dohnal, M. Hejduk, R. Plasil, and J. Glosík, J. Phys. Chem. A (2013), doi: 10.1021/jp311978n.
[24] M. R. Mahdavi, J. B. Hasted, and M. M. Nakshbandi, J. Phys. B **4**, 1726 (1971).
[25] D. Smith, N. G. Adams, A. G. Dean, and M. J. Church, J. Phys. D: Appl. Phys. **8**, 141 (1975).
[26] J. Glosik, G. Bano, R. Plasil, A. Luca, and P. Zakouril, Int. J. Mass Spectrom. **189**, 103 (1999).
[27] A. J. Yencha, in *Electron Spectroscopy: Theory, Techniques and Applications*, edited by C. R. Bundle and A. D. Baker (Academic Press, London, 1984), Vol. 5.
[28] R. Plasil, I. Korolov, T. Kotrik, P. Dohnal, G. Bano, Z. Donko, and J. Glosik, Eur. Phys. J. D **54**, 391 (2009).
[29] I. Korolov, T. Kotrik, R. Plasil, J. Varju, M. Hejduk, and J. Glosik, Contrib. Plasma Phys. **48**, 521 (2008).
[30] J. D. Swift and M. J. R. Schwar, *Electrical Probes for Plasma Diagnostics* (Elsevier, New York, 1969).
[31] O. Chudacek, P. Kudrna, J. Glosik, M. Sicha, and M. Tichy, Contrib. Plasma Phys. **35**, 503 (1995).
[32] P. Macko, G. Bano, P. Hlavenka, R. Plasil, V. Poterya, A. Pysanenko, O. Votava, R. Johnsen, and J. Glosik, Int. J. Mass Spectrom. **233**, 299 (2004).

[33] O. Novotny, R. Plasil, A. Pysanenko, I. Korolov, and J. Glosik, J. Phys. B **39**, 2561 (2006).
[34] R. Plasil, J. Glosik, V. Poterya, P. Kudrna, J. Rusz, M. Tichy, and A. Pysanenko, Int. J. Mass Spectrom. **218**, 105 (2002).
[35] D. R. Bates, Proc. R. Soc. London, Ser. A **337**, 15 (1974).
[36] D. K. Bohme, D. B. Dunkin, F. C. Fehsendeld, and E. E. Ferguson, J. Chem. Phys. **51**, 863 (1969).
[37] B. M. Smirnov, Sov. Phys. Usp. **20**, 119 (1977).
[38] J. Royal and A. E. Orel, Phys. Rev. A **73**, 042706 (2006).
[39] J. L. McLain, V. Poterya, C. D. Molek, L. M. Babcock, and N. G. Adams, J. Phys. Chem. A **108**, 6704 (2004).
[40] E. Alge, N. G. Adams, and D. Smith, J. Phys. B **16**, 1433 (1983).
[41] F. L. Walls and G. H. Dunn, J. Geophys. Res. **79**, 1911 (1974).
[42] R. Johnsen, Int. J. Mass Spectrom. Ion Processes **81**, 67 (1987).
[43] N. G. Adams, D. Smith, and E. Alge, J. Chem. Phys. **81**, 1778 (1984).
[44] R. Peverall, S. Rosen, J. R. Peterson, M. Larsson, A. Al-Khalili, L. Vikor, J. Semaniak, R. Bobbenkamp, A. N. Maurellis, and W. J. van der Zande, J. Chem. Phys. **114**, 6679 (2001).
[45] P. Spanel, L. Dittrichova, and D. Smith, Int. J. Mass Spectrom. **129**, 183 (1993).
[46] E. Mason and E. McDaniel, *Transport Properties of Ions in Gases* (Wiley, New York, 1988).
[47] L. Viehland, A. Viggiano, and E. Mason, J. Chem. Phys. **95**, 7286 (1991).
[48] W. Lindinger and D. Albritton, J. Chem. Phys. **62**, 3517 (1975).
[49] R. Johnsen and M. A. Biondi, Phys. Rev. A **20**, 221 (1979).
[50] J. Berlande, M. Cheret, R. Deloche, A. Gonfalone, and C. Manus, Phys. Rev. A **1**, 887 (1970).
[51] R. J. van Sonsbeek, R. Cooper, and R. N. Bhave, J. Chem. Phys. **97**, 1800 (1992).
[52] T. Kotrik, P. Dohnal, I. Korolov, R. Plasil, S. Roucka, J. Glosik, C. H. Greene, and V. Kokoouline, J. Chem. Phys. **133**, 034305 (2010).